Query Form

Journal: SREP

Author: The following queries have arisen during the editing of your manuscript. Please answer queries by making the requisite corrections at the appropriate positions in the text.

Query	Details Required	Author's Response
AQ1	Please check and confirm the author names and initials are correct. Also, kindly confirm the details in the metadata are correct.	

scientific reports

OPEN

Dynamical phase diagram of the quantum Ising model with cluster interaction under noiseless and noisy driven field

S. Kheiri[1,2], **R. Jafari**[1,3✉], **S. Mahdavifar**[2], **E. Nedaaee Oskoee**[1] & **A. Akbari**[4]

AQ1

In most lattice models, gap closing typically occurs at high-symmetry points in the Brillouin zone. In the transverse field Ising model with cluster interaction, the gap closes at high-symmetry points, as well as at the phase transition between paramagnetic and cluster phases, where the gap-closing mode can be moved by tuning the strength of the cluster interaction. We take advantage of this property to examine the nonequilibrium dynamics of the model in the framework of dynamical quantum phase transitions (DQPTs) after a noiseless and noisy ramp of the transverse magnetic field. The numerical results show that DQPTs always happen if the starting or ending point of the quench field is restricted between two critical points. In other ways, there is always critical sweep velocity above which DQPTs disappear. Our finding reveals that noise modifies drastically the dynamical phase diagram of the model. We find that the critical sweep velocity decreases by enhancing the noise intensity and scales linearly with the square of noise intensity for weak and strong noise. Moreover, the region with multi-critical modes (MCMs) induced in the dynamical phase diagram by noise. The sweep velocity under which the system enters the MCMs region increases by enhancing the noise and scales linearly with the square of noise intensity.

Developing a comprehensive theoretical framework for nonequilibrium phenomena is a challenging problem in physics with an impact vastly surpassing this specific discipline[1–5]. A systematic understanding is crucial for many different areas such as many-body correlations[6,7], quantum matter[8,9], quantum simulations[10,11], and quantum technologies,[12,13], which require the control of many-body physical systems at the quantum level. This question has recently promoted experimental and theoretical studies of the out-of-equilibrium dynamics of many-body systems[14–16].

Recent experimental advances in synthesizing various quantum platforms, including ultra-cold atoms in optical lattices[17–21], trapped ions[22–25], nitrogen-vacancy centers in diamond[26], superconducting qubit systems[27], and quantum walks in photonic systems[28,29], provide a framework for experimentally studying the out-of-equilibrium dynamics of many-body systems. Nevertheless, the simulation of the adapted time dependent Hamiltonian in any real experiment is imperfect and noisy fluctuations are imminent. In other words, the noises are ubiquitous and imperative in any physical system and the stability of a dynamical system can be strongly affected in the presence of uncontrolled perturbations such as random noise[30–33].

Consequently, understanding the effect of noise on Hamiltonian evolution is crucial for correctly predicting the results of experiments and designing experimental setups robust against the effects of noise[34].

Within this context, we investigate the effects of Gaussian white noise on the dynamical quantum phase transitions (DQPTs). Dynamical quantum phase transitions have become one of the focal points in the study of quantum matter out of equilibrium[35–37]. DQPT was theoretically proposed in nonequilibrium quantum systems, inspired by the concept of nonanalyticities associated with the free-energy density of a classical system at a finite-temperature transition. The DQPT is signaled through the nonanalytical behavior of dynamical free energy[38–52], where real time plays the role of the control parameter[53–62]. DQPT displays a phase transition between dynamically emerging quantum phases that takes place during the nonequilibrium coherent quantum time evolution under sudden quench and ramp protocols[63–83] or time-periodic modulation of Hamiltonian[26,84–90].

[1]Department of Physics, Institute for Advanced Studies in Basic Sciences (IASBS), Zanjan 45137-66731, Iran. [2]Department of Physics, University of Guilan, Rasht 41335-1914, Iran. [3]School of Quantum Physics and Matter, Institute for Research in Fundamental Sciences (IPM), Tehran 19538-33511, Iran. [4]Beijing Institute of Mathematical Sciences and Applications (BIMSA), Huairou District, Beijing 101408, China. ✉email: raadmehr.jafari@gmail.com

It has been also established that there exists a dynamical topological order parameter (DTOP), similar to the order parameters at conventional quantum phase transition, which uncover DQPTs[91,92]. The presence of DTOP, which takes integer values as a function of time and jumps at the critical times, represents the emergence of a topological characteristic associated with the time evolution of nonequilibrium systems. Theoretical predictions of DQPT were confirmed experimentally in several studies[21–23,27,28,93,94]. Most of the research dedicated to deterministic quantum evolution induces by sudden quench or ramp of the Hamiltonian parameters. However, inadequate consideration has been associated with the stochastic driving of thermally isolated systems with noisy Hamiltonian[95–101].

In this work we study DQPTs in the one-dimensional quantum Ising model with cluster interaction (three site spin)[102–111] in the presence of the noiseless and noisy linear driven transverse field. The cluster interaction is generated in the first step of a real space renormalization group procedure[108]. In most lattice models, the gap closing typically occurs at the edges or center of the Brillouin zone (high-symmetry points). In the time-independent transverse field Ising model with cluster interactions, beside the gap closing at the high-symmetry points in the Brillouin zone, the gap closing occurs at the quantum phase transition between the paramagnetic and cluster phases of the model which can be moved by tuning the cluster interaction strength.

Moreover, the cluster interaction breaks the usual symmetry of the transverse field Ising model phase diagram. We take advantage of this property to explore the nonequilibrium dynamics of the model using the notion of DQPTs following the noiseless and noisy ramping of the transverse field. The phase diagram symmetry breaking is dramatic, as the DQPTs features are distinct for ramp down and ramp up of the transverse magnetic field.

We show that, when the ramp field crosses the critical points (does not matter how many QCPs are crossed) there exist a critical sweep velocity above which DQPTs are whipped out, if the starting or ending point of the ramp field is not confined between two critical points. Otherwise, DQPTs always occur even for a sudden quench case. In addition, we discover that the sweep velocity above which DQPTs disappear decreases by enhancing the noise intensity and scales linearly with the square of noise intensity for both weak and strong noise, which support our previous observation[112].

Further, noise induces MCMs region (continuous critical time) in the dynamical phase diagram of the model. The numerical results show that the sweep velocity below which the system enters the MCMs region enhances by increasing the noise intensity and also scales linearly with the square of noise intensity.

The paper is organized as follows. In Sect. 2, the dynamical free energy and dynamical topological order parameter of the two level Hamiltonians are discussed. In Sect. 3, we introduce the model along with its exact solution and equilibrium phase diagram. Section 4 is dedicated to the numerical simulation of the noiseless case based on the analytical result. Section 5 focuses on the numerical simulation of the model utilizing the exact noise master equation. Section 6 contains some concluding remarks.

Ramp protocol in an integrable model
Dynamical free energy
We adopt the terminology used in Refs.[77,95,113] for all ramp schemes, which will be examined in the discussions that follow. Suppose we have an integrable model that can be reduced to a two-level Hamiltonian, denoted as $H_k(h)$, for each momentum mode k. At the initial time ($t_i \to -\infty$), the system is in the ground state $|\alpha_k^i\rangle$ of the pre-quench Hamiltonian $H_k(h_i)$ for each mode. In the ramp protocol, the Hamiltonian is described by a parameter h, varies from an initial value h_i at time t_i, following the linear time driven scheme $h(t) = vt$, to a final value h_f at time t_f (Fig. 1). This is designed so that the system crosses the quantum critical point (QCP) at $h = h_c$. Crossing the critical point (gap closing point) disrupts the adiabatic condition, leading to a non-adiabatic transition. Therefore the final state $|\psi_k(h_f)\rangle = |\psi_k^f\rangle$ (corresponding to the k-th mode) may not be the ground state of the post-quench Hamiltonian $H_k(h_f) = H_k^f$.

Consequently, the final state should be given as a linear combination of the ground and excited states $|\psi_k^f\rangle = a_k|\alpha_k^f\rangle + b_k|\beta_k^f\rangle$, ($|a_k|^2 + |b_k|^2 = 1$) where, $|\alpha_k^f\rangle$ and $|\beta_k^f\rangle$ are the ground and the excited states of the post-quench Hamiltonian H_k^f, respectively with the corresponding energy eigenvalues $\epsilon_{k,1}^f$ and $\epsilon_{k,2}^f$.

The probability of non-adiabatic transition resulting in the system being in the excited state at $h = h_f$ is represented as $p_k = |b_k|^2 = |\langle \beta_k^f|\alpha_k^i\rangle|^2$. Consequently, the Loschmidt overlap and the associated dynamical free energy[35,37], for mode k at $t > t_f$ are specified by[77,95,113]
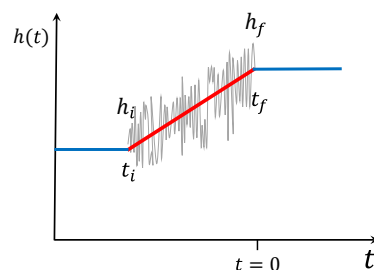

Fig. 1. A schematic representation of a linear ramp protocol accompanied by noise fluctuations. The quenching process starts at $t_i < 0$ with the magnetic field $h(t)$ set to h_i and ends at t_f, where $h(t_f) = h_f$.

$$\mathcal{G}_k = \langle \psi_k^f | \exp(-iH_k^f t) | \psi_k^f \rangle = |a_k|^2 \exp(-i\epsilon_{k,1}^f t) + |b_k|^2 \exp(-i\epsilon_{k,2}^f t),$$

$$g(t) = -\frac{1}{N} \sum_k g_k(t), \quad g_k(t) = \ln |\mathcal{G}_k|^2 \tag{1}$$

respectively, where N is the size of the system.

By summing the contributions from all modes and substituting the summation with an integral in the thermodynamic limit, one obtains[77,95,113,114]

$$g(t) = -\frac{1}{2\pi} \int_0^{\pi} \ln\left(1 + 4p_k(p_k - 1)\sin^2\left(\frac{\epsilon_{k,2}^f - \epsilon_{k,1}^f}{2}\right)t\right) dk \tag{2}$$

where the parameter t is defined as the time elapsed since the final state, $|\psi_k^f\rangle$, is achieved at the end of the ramp process (Fig. 1). The non-analyticities in $g(t)$ occur at the values of the real time $t_n^* s$ given by

$$t_n^* = \frac{\pi}{\epsilon_{k^*,2}^f - \epsilon_{k^*,1}^f}(2n + 1) \tag{3}$$

These are the critical times for the DQPTs, with k^* the mode at which the argument of the logarithm in Eq. (2) vanishes for $|b_{k^*}|^2 = p_{k^*} = 1/2$. For the case $\epsilon_{k^*,2}^f = -\epsilon_{k^*,1}^f = \epsilon_{k^*}^f$, Eq. (3) is simplified to

$$t_n^* = t^*\left(n + \frac{1}{2}\right), \quad t^* = \frac{\pi}{\epsilon_{k^*}^f} \tag{4}$$

In the following section, we revisit the phase diagram and exact solution of the one-dimensional transverse field Ising model with three spin interacting and also the noiseless DQPT.

Model and exact solution

The Hamiltonian system under investigation arises from hybridisation between quantum statistical mechanics with quantum computation. A reference system is established using cold atoms in a triangular optical lattice[116]. With an appropriate selection of parameters, this system can be modeled as a spin system exhibiting a specific ring-exchange interaction within the triangular lattice, which can subsequently be transformed into a "zig-zag chain". This setup creates a physical platform for a one-way route to quantum computation, where the algorithm involves specific measurements aimed at reconstructing the high degree of entanglement characteristic of the cluster state[117]. Interestingly, in addition to the three-spin ring-exchange interaction, various two-spin interactions can emerge in the system. Therefore, the cluster interaction competes with the exchange interaction by tuning a control parameter[103,105–107,109,118,119].

The Hamiltonian of linear time dependent transverse field Ising model with cluster interaction[105,107] is given as

$$H(t) = -J \sum_{j=1}^{N} \sigma_{j-1}^z \sigma_j^z - J_3 \sum_{j=1}^{N} \sigma_j^x \sigma_{j-1}^z \sigma_{j+1}^z - h(t) \sum_{j=1}^{N} \sigma_j^x, \tag{5}$$

where σ_j^α $(\alpha = x, z)$ represents the Pauli matrices that act on site j for a chain of length N with periodic boundary conditions (PBC) ($\sigma_{N+1}^\alpha = \sigma_1^\alpha$), J denotes the strength of the nearest neighbor ferromagnetic interaction, J_3 indicates the strength of the three-spin interaction, and the transverse field $h(t) = h_f + vt$ ramping up from the initial value $h_i < 0$ at time $t = t_i < 0$ to the final values h_f at $t_f \to 0^-$, with sweep velocity v (Fig. 1). For $J_3 = 0$, the model reduces to the well-known transverse field Ising model.

By performing the Jordan-Wigner transformation[120,121]

$$\sigma_j^z = -\prod_{j=1}^{j-1} \sigma_j^x \left(c_j^\dagger + c_j\right), \quad \sigma_j^x = 1 - 2c_j^\dagger c_j,$$

and applying the Fourier transformation $c_j = (e^{-i\pi/4}/\sqrt{N}) \sum_k \exp(-ikj)c_k$, the Hamiltonian of Eq. (5) can be expressed as the sum of $N/2$ non-interacting terms, i.e., $H(t) = \sum_{k>0} H_k(t)$, with

$$H_k(t) = A(k, t)\left(c_k^\dagger c_k - c_{-k}c_{-k}^\dagger\right) + B(k)\left(c_{-k}c_k + c_k^\dagger c_{-k}^\dagger\right),$$

where $A(k, t) = 2(h(t) - J\cos k - J_3 \cos 2k)$ and $B(k) = 2(J\sin k + J_3 \sin 2k)$, and the summation over k is limited to positive k values in the form $k = (2n-1)\pi/N$ with $n = 1, ..., N/2$. The Bloch single particle Hamiltonian $H_k(t)$ can be expressed as:

$$H_k(t) = \begin{pmatrix} A(k, t) & B(k) \\ B(k) & -A(k, t) \end{pmatrix}, \tag{6}$$

with the instantaneous eigenvalues and eigenstates

$$
\begin{aligned}
\varepsilon_k^\pm(t) &= \pm\,\varepsilon_k(t) = \pm\sqrt{A^2(k,t)+B^2(k)}, \\
|\alpha_k(t)\rangle &= \sin(\theta_k(t))|\uparrow\rangle - \cos(\theta_k(t))|\downarrow\rangle, \\
|\beta_k(t)\rangle &= \cos(\theta_k(t))|\uparrow\rangle + \sin(\theta_k(t))|\downarrow\rangle,
\end{aligned}
\tag{7}
$$

where

$$
\sin(\theta_k(t)) = \sqrt{\frac{1}{2}\left(1 - \frac{A(k,t)}{\varepsilon_k(t)}\right)}, \quad \cos(\theta_k(t)) = \sqrt{\frac{1}{2}\left(1 + \frac{A(k,t)}{\varepsilon_k(t)}\right)}.
$$

Without loss of generality we set $J = 1$ as the energy scale and $J_3 > 0$. For the time independent case ($h(t) = h$), the equilibrium phase diagram of the model can be constructed by identifying the regions of quantum criticality where the system becomes gapless in the thermodynamic limit ($N \to \infty$). It can be shown that the gap of spectrum vanishes at $h_c^{(1)} = J_3 - 1$ and $h_c^{(2)} = J_3 + 1$, with ordering wave vectors $k = \pi$ and $k = 0$, respectively. These two lines correspond to the quantum phase transitions from a quantum paramagnetic phase to a ferromagnetically ordered phase with the associated exponents being the same as the transverse field Ising model[122]. Moreover, there is an additional gap closing point at $h_c^{(a)} = -J_3$. This transition belongs to the universality class of the anisotropic transition observed in the transverse XY model dual to the Hamiltonian in Eq. (5)[123]. The phase boundary is surrounded by the incommensurate phases on either side with wave vector given by

$$
k_a = \arccos\left((J_3 - h)/4hJ_3\right).
\tag{8}
$$

Obviously, for $J_3 \leq 1/2$, the anisotropic phase transition can not occur. The equilibrium phase diagram of the model is depicted in Fig. 2. We will exploit an intriguing feature of the model: the movability of the gap-closing mode in the Brillouin zone, controllable by tuning the cluster interaction, to uncover the aspects of DQPTs, under linear time driven magnetic field.

The time-dependent Schrödinger equation of the Hamiltonian Eq. (6) with the linear time dependent transverse field, can be transformed into the Landau-Zener (LZ) problem (see Supplemental Material Sect. 1) which is exactly solvable[124,125]. If the system prepared initially in its ground state at $h_i = -10$ ($t_i \to -\infty$), the probability of the k:th mode being in the excited state at a finite time t is determined by the non-adiabatic transition probability[124] (see Supplemental Material Sect. 1).

$$
p_k(\tau) = e^{\pi\gamma^2/2v}\left|\mathcal{D}_{i\gamma^2/v}\left(\sqrt{v}e^{3i\pi/4}\tau\right)\cos(\theta_k(\tau)) - \frac{\gamma}{\sqrt{v}}e^{-i\pi/4}\mathcal{D}_{-1+i\gamma^2/v}\left(\sqrt{v}e^{3i\pi/4}\tau\right)\sin(\theta_k(\tau))\right|^2
\tag{9}
$$

where $\tau = 2(vt - \cos k - \lambda_2\cos 2k)/v$, and $\gamma = B_k/2$, and $\mathcal{D}_\nu(z)$ is the parabolic cylinder function[126,127]. Furthermore, as $t_f \to +\infty$ ($h_f \gg h_c$), the probability of excitations p_k, is represented by the LZ transition probability,

$$
p_{LZ} = e^{-2\pi\gamma^2/v}.
\tag{10}
$$

In the following section, we will study the dynamical phase diagram of the model for the passage of the noiseless transverse field through the critical points.
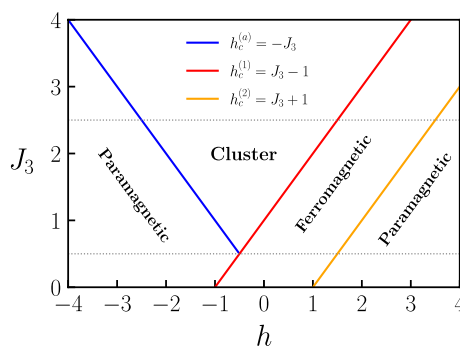

Fig. 2. (Color online) The equilibrium phase diagram of the Ising model with cluster interaction. The blue line indicates the anisotropy transition which takes place between the paramagnetic and cluster phases. The red and yellow lines, represent the Ising like transition points. The black dashed lines indicate $J_3 = 1/4$ and $J_3 = 5/2$ as reference lines to enhance the illustration of the critical points at $h = -1/2$ and $h = 3/2$.

Noiseless numerical results

The results of our numerical simulations, conducted using an analytical approach, are presented in this section to analyze the dynamics of the model through the concept of DQPTs. For this aim, we consider three cases of the noiseless ramp protocol through the single, two and three critical points for quenches starting at $h_i = -10$.

Quench across a single critical point ($h_f = -1/2$)

When time driven magnetic field crosses a single critical point, i.e, $h_f = -1/2$, we consider two cases $J_3 < 1/2$ and $J_3 > 1/2$, respectively.

 (i) In the case that $J_3 < 1/2$, the ramp field crosses the Ising type single critical point $h_c^{(1)}$, at $k_c = \pi$, and the probability of excitation p_k, depends on the value of *k*. As expected, when the system crosses the critical point, it undergoes non-adiabatic evolution due to the gap closing and yields maximum transition probability at the gap closing mode $p_{k=\pi} = 1$. Nevertheless, far away from the gap closing mode, the system evolves adiabatically due to the non-zero energy gap and leads to small transition probability ($p_{k=0} \to 0$). Given these two cases and continuity of the transition probability as a function of allowed mode *k* in the thermodynamic limit, implies that **there exist a critical mode** k^* **at which** $p_{k^*} = 1/2$ **and consequently DQPTs always occur** for a quench crosses a single critical point. The numerical simulation of transition probability has been plotted in Fig. 3(a) versus *k* for $h_f = -1/2$ and $J_3 = 1/4$, for various sweep velocities as the ramp field passes through the single critical point $h_c = -3/4$. As seen, for a quench that crossing a single critical point, there is always a critical momenta k^* and consequently those of t_n^*, given by Eq. (4).

 (ii) In the case that $J_3 > 1/2$, the ramp transverse field crosses the single anisotropic transition point $h_c^{(a)}$, where the band gap closes inside the Brillouin zone at k_a given by Eq. (8). At this critical point, the system undergoes a phase transition from the paramagnetic phase to the cluster phase. We expect that, the system experiences non-adiabatic transition at the gap closing mode, i.e., $p_{k_a} = 1$, and evolves adiabatically away from the gap closing mode ($p_{k=0,\pi} \to 0$). Since the gap closing occurs at interval $0 < k_a < \pi$, expected that two critical modes emerge in the system at which $p_{k^*} = 1/2$. Figure 3(b) displays the transition probability versus *k* for $J_3 = 1$ and $h_f = -1/2$, as the ramp field passages across the single critical point
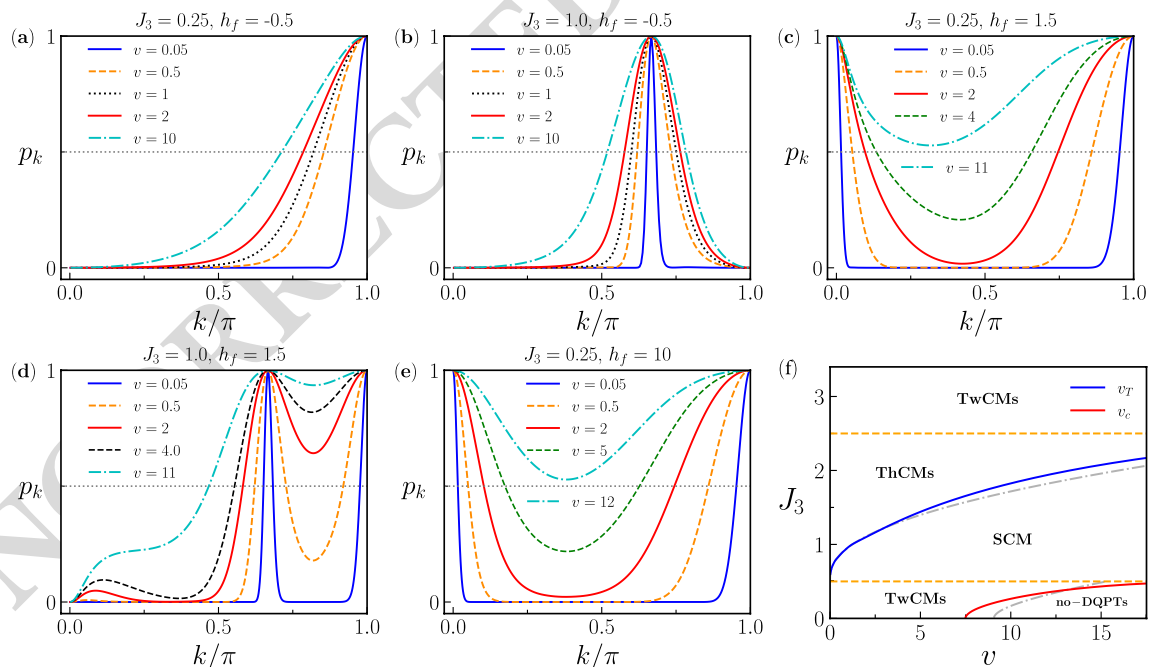

Fig. 3. (Color plot) The transition probability p_k following the quench from the initial value of transverse field $h_i = -10$ to the various values of quench field end h_f for various sweep velocities. (**a**) for $J_3 = 1/4$ and $h_f = -0.5$ where the ramped quench crosses a single Ising like quantum critical point $h_c^{(1)} = -3/4$, (**b**) for $J_3 = 1$ and $h_f = -0.5$ where the ramped quench crosses single quantum critical points $h_c^{(a)} = -1$, (**c**) for $J_3 = 1/4$ and $h_f = 1.5$ where the quench crosses two Ising like quantum critical points $h_c^{(1)} = -3/4$, and $h_c^{(1)} = 5/4$ (**d**) for $J_3 = 1$ and $h_f = 1.5$ where the ramped quench crosses two quantum critical points $h_c^{(a)} = -1$ and $h_c^{(1)} = 0$, (**e**) for $J_3 = 1$ and $h_f = 10$, where the ramped quench crosses three quantum critical points $h_c^{(a)} = -1$, $h_c^{(1)} = 0$, and $h_c^{(2)} = 2$. (**f**) The dynamical phase diagram of the model in the $(J_3; v)$ plane in the absence of the noise for a quench from $h_i = -10$ to $h_f = 1.5$. The diagram is divided into three regions. The horizontal yellow dashed-dotted line represents $J_3 = 1/2$ and $J_3 = 5/2$. The blue solid line separates two regions where the system shows SCM and ThCMs. The red solid line shows the boundary between regions characterized by TwCMs and those with no-DQPTs. The blurred gray dashed-dotted curves represent the boundaries obtained from LZ transition formula.

$h_c = -1$ where the band gap closes at $k = 2\pi/3$. As seen, there are two critical modes k_α^* and k_β^* at which $p_{k_\alpha^*} = p_{k_\beta^*} = 1/2$. In other words, if the quench crosses a single critical point at which the energy gap closes inside the Brillouin zone, the system reveals two critical modes at which DQPTs happen. While, for a quench that crossing a single critical point where the gap closing occurs at high-symmetry points in the Brillouin zone ($k = 0, \pi$)[77,113], the system includes only a single critical mode (similar to Fig. 3a).

Quench across the two critical points ($h_f = 3/2$)
For a quench crosses two critical points, i.e, $h_f = 3/2$, we have considered once again two cases $J_3 < 1/2$ and $1/2 < J_3 < 5/2$, respectively. It should be mentioned that, for $h_f = 3/2$ and $J_3 > 5/2$, the quench transverse field crosses only a single anisotropic transition point and the dynamics of the system is similar to that of discussed in previous Sect. (4.1-(ii)).

Comparing these two cases reveals that the modes confined between two gap closing modes, can be easily excited to the upper level for large sweep velocity. However, the modes which do not restricted between two modes with maximum transition probability ($p_k = 1$), prefer to stay at the lower level even for a sudden quench case. Although in both cases the quench field crosses two critical points, neither starting point nor ending point of the ramp field is confined between two critical point for $J_3 < 1/2$ case. While for $J_3 > 1/2$ case, ramp field end is restricted between two critical points. Therefore, we come to the conclusion that, DQPTs are always present if starting or ending point of the quench field is restricted between two critical points, even for sudden quench case. Otherwise, there is critical sweep velocity above which DQPTs are wiped out.

Quench across the three critical points ($h_f = 10$)
To perform a quench across three critical points, the quench field end should be larger than $h_c^{(2)}$ and the cluster interaction $J_3 > 1/2$. In such a case, the quench field is swept from one equilibrium paramagnetic phase to another one and passage through the critical points $h_c^{(a)}$, $h_c^{(1)}$ and $h_c^{(2)}$ where the band gap closes at $k = k_a$, $k = \pi$ and $k = 0$. Thus, the transition probability is maximum at $k = k_a$, $k = \pi$ and $k = 0$ and p_k discloses two minimum between three gap closing modes. Appearance of DQPTs is required that the minimums of p_k becomes less than 1/2. In this case, the system encompasses four critical modes (FCMs) and DQPTs is wiped out for a sweep velocity above the critical sweep velocity. Moreover, we expect that the system shows transition from FCMs case to two critical modes case for sweep velocity smaller than the critical sweep velocity.

For $h_f \gg h_c^{(2)}$, the transition probability is given as LZ transition probability and the critical sweep velocity above which DQPTs disappear can be obtained analytically. As mentioned, DQPTs appear if the condition $p_{LZ}^{min} \leqslant 1/2$ is satisfied. It is straightforward to show that, two minimum of the transition probability occurs at $k = k_m^\pm = \arccos((-J \pm \sqrt{J^2 + 32J_3^2})/8J_3)$. More analysis manifest that, the minimum at k_m^+ is the global minimum of transition probability while the minimum at k_m^- is the local minimum. Consequently, if both global and local minimums of p_k are less than 1/2 the system illustrates FCMs which yielding DQPTs. Further, the transition from FCMs case to two critical modes case occurs if the local minimum of p_k is greater than 1/2 while DQPTs are removed if the global minimum exceed 1/2.

Detailed analysis shows that, the condition $p_{k_m^+} \leqslant 1/2$ is satisfied if $v \leqslant v_c$ with $v_c = 2\pi(\gamma_m^g)^2/\ln(2)$ where $\gamma_m^g = J \sin k_m^+ + J_3 \sin 2k_m^+$ which results DQPTs. In addition, **the system transits from FCMs case to two critical modes case for a sweep velocity** $v > v_{FT} = 2\pi(\gamma_m^\ell)^2/\ln(2)$ where $\gamma_m^\ell = J \sin k_m^- + J_3 \sin 2k_m^-$.

The transition probability has been shown in Fig. 3(e) versus k, for $h_f = 10$ and $J_3 = 1$. As seen, p_k represents two minimum at $k_m^+/\pi = 0.299$ and $k_m^-/\pi = 0.819$, and for sufficient slow sweep velocity system unveils FCMs at which $p_{k^*} = 1/2$. As the sweep velocity increases, the transition probability at $k_m^\pm$ enhances and $p_{k_m^-}$ exceeds 1/2 at $v_{FT} = 1.234$, and hence system enters two critical modes case. Further increase of sweep velocity raises also the transition probability at global minimum $\left(p_{k_m^+}\right)$ and DQPTs are wiped out for

$v > v_c = 28.084$.

As clear, for a quench crossing three critical points where the end of quench does not limited between two critical points, the system reveals critical sweep velocity above which DQPTs are disappeared. This behaviour is also observed for a quench that crossing two critical points for $J_3 < 1/2$, where the ramp field end does not confined between two critical point (4.1-(i)).

Dynamical phase diagram
In Fig. 3(f), the dynamical phase diagram of the model has been displayed in $v - J_3$ plane for $h_f = 1.5$. The dynamical phase diagram represents dynamics of the system for three cases of quench: crosses two critical points where quench field end does not confined between two critical points ($J_3 < 1/2$), across two critical points where quench field end limited between two critical points ($1/2 < J_3 < 5/2$) and passage through a single anisotropic transition ($J_3 > 5/2$). The phase diagram discloses five distinct regions, no-DQPTs, single critical modes (SCM), two critical modes (TwCMs) and three critical modes (ThCMs). As seen, for $J_3 < 1/2$ where the quench crosses two Ising like transition points ($h_c^{(1)}, h_c^{(2)}$) and the end of quench is not restricted between two critical points ($h_f > h_c^{(2)}$), the system reveals critical sweep velocity (red solid line) above which DQPTs are disappeared. While for $v < v_c$ system experiences DQPTs with two critical modes. For $1/2 < J_3 < 5/2$ although the quench passage through two critical points, the ramp field end is confined between two critical points ($h_c^{(1)} < h_f < h_c^{(2)}$) and DQPTs always are present. In such a case, the system encloses three critical modes region which passes to single critical mode for $v > v_T$ (blue solid line). As J_3 exceeds 5/2 the quench from $h_i = -10$ to $h_f = 1.5$ crosses only a single anisotropic transition point ($h_c^{(a)}$) which displays two critical modes.

Figure 4 represents the dynamical phase diagram of the model in the $v - J_3$ plane for the quench to $h_f = 10$, which crosses two critical points for $J_3 < 1/2$ and passage through three critical points for $J_3 > 1/2$. As seen, the dynamical phase diagram contains three distinct regions: FCMs, two critical modes (TwCMs), and no-DQPTs regions. The red solid line in the dynamical phase diagram indicates the critical sweep velocity (v_c) which separates no-DQPTs region from two critical modes region. The blue dashed-dotted line represents v_T under which the system enters FCMs region which appears only for $J_3 > 1/2$ where quench pass over three critical points.

From these observations, we come to the conclusion that, DQPTs always happen if the starting or ending point of the ramp field confined between two critical point, even for sudden quench case. While for a quench that starting or ending point of the ramp field does not restricted between two critical points, there exist critical sweep velocity above which DQPTs are wiped out.

Noisy ramp quench

As noted, noise is an unavoidable and inescapable in any physical system. Consequently, comprehending the exact effects of noise is crucial in both classical and quantum contexts[95–99,128–130]. Noise introduces randomness into the system, thereby disrupting coherent evolution. In this section, we investigate DQPTs in the one-dimensional quantum Ising model with cluster interaction, following a ramp protocol with fluctuations. To this end, we add uncorrelated Gaussian noise to the time dependent transverse field, expressed as $h(t) = h_f + vt + R(t)$, where $R(t)$ represents a random fluctuation confined to the ramp interval $[t_i, t_f = 0[$, with a vanishing mean, $\langle R(t) \rangle = 0$. We use white noise with Gaussian two-point correlations $\langle R(t)R(t') \rangle = \xi^2 \delta(t - t')$ where ξ characterizes the strength of the noise (ξ^2 has units of time). It should be mention that, the state of system at the end of noisy ramp is mixed state (an ensemble of pure states) and has been shown that DQPTs disappear in the presence of noise[95]. Although it is feasible to construct a pure state in the experiment, creating a mixed state experimentally is not practical. Therefore, to investigate the impact of noise on DQPTs in an experimental setting, we have assumed the system's state at $t = t_f$ to be the noise-averaged pure state i.e., $|\psi(t_f)\rangle = \sqrt{1 - p_k}|\alpha_k(t_f)\rangle + \sqrt{p_k}|\beta_k(t_f)\rangle$, and the dynamical free energy is obtained based on this presumption; thus, the trustworthiness of our findings depends on this assumption.

To determine the transition probability in the presence of noise, we solve numerically the exact noise master equation[95,96,131–134] for the averaged density matrix $\rho_k(t)$ of the Hamiltonian which includes noise $H_k^{(\xi)} = H_k^{(0)}(t) + R(t)H_1$; where $H_k^{(0)}(t)$ denotes noiseless Hamiltonian and $R(t)H_1 = 2R(t)\sigma^z$ represents the added noise which appears during the ramp process where $t \in [t_i = h_i/v, t_f = 0)$ and the system prepared in its ground state at $t = t_i$. The exact noise master equation in the presence of the uncorrelated Gaussian noise is given as follows[95–98,128]

$$\frac{d}{dt}\rho_k(t) = -i\Big[H_k^{(0)}(t), \rho_k(t)\Big] - \frac{\xi^2}{2}\Big[H_1, \big[H_1, \rho_k(t)\big]\Big] \tag{11}$$

By numerically solving the master equation, the transition probability in the presence of uncorrelated Gaussian noise is given as[95–99]

$$p_k = \langle\beta_k(t_f)|\rho_k(t)|\beta_k(t_f)\rangle. \tag{12}$$

where, $|\beta_k(t_f)\rangle$ is the excited state of the system at the end of quench (Eq. 7). The dynamical phase diagram of the model is characterized by the interplay of the near-adiabatic dynamics of the system's gapped fermionic modes and the accumulation of noise-induced excitations during the evolution. Moreover, we expect that large values of the sweep velocity gives less time for the noise to be effective. In this section we have searched the effects of noise on transition probability and dynamical phase diagram of the model.

Transition probability

Without loss of generality and prevent complexity we suppose that in the presence of the noise $h(t)$ altering from $h_i = -10$ to $h_f = 10$, which crosses all critical points. Therefore, the quench field end is not blocked between two critical points and the system shows transition from DQPTs region to no-DQPTs region. From a physical point of view, the influence of noise on transition probability and critical sweep velocity is an interesting open
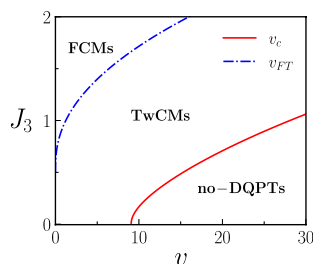

Fig. 4. (Color online) The dynamical phase diagram of the model in the $(J_3; v)$ plane for a quench from $h_i = -10$ to $h_f = 10$ in the absence of the noise.

question: Will noise reduce or enhance the critical sweep velocity or are DQPTs always possible? particular, we wish to determine how the dynamical phase diagram of the model is modified in the presence of noise.

Figure 5 illustrates the transition probability as a function of k for different values of sweep velocities and noise intensity for $J_3 = 1/4$ and $J_3 = 1$. As observed, for $\xi/v \ll 1$, the effect of noise is to displace the critical mode k^*, resulting in a sequence of DQPTs. The gradual increase in noise intensity, the effect of noise turns in an unanticipated direction for $\xi/v \sim \mathcal{O}(1)$. In such a case, p_k curve is locked to the value 1/2 over a finite interval of momenta, leads to MCMs. This suggests that the noise behaves like a high-temperature source, leading to maximally mixed states unless the k-modes are too "light" (easily excited to the upper level by the Kibble-Zurek Mechanism[97]).

Moreover, the main effect of noise during ramping time is that the inequality $p_{k_m}^{min} < 1/2$ fulfilled only for sufficiently low noise amplitudes. In other words, very strong noise ($\xi/v \gg 1$) leads to non-adiabatic transitions of such high probability that a maximally mixed state ($p_k = 1/2$) is not observed at the end of quench, consequently preventing the emergence of DQPTs even for $v < v_c$. Therefore, the boundary between "DQPTs" and "no-DQPTs" regions is changed in the presence of noise. In the following, we will explore the dynamical phase diagram of the model for different noise intensity to clarify the process of noise effects on DQPTs.

Dynamical phase diagram and scaling of critical sweep velocity

The phase diagram of the model in the presence of noise has been plotted in Fig. 6(a)–(f) in $v - \xi$ plane for $J_3 = 1/4$ and $J_3 = 1.2$. The numerical results indicate that, in the presence of noise the critical sweep velocity ($v_c^{(\xi)}$) above which the DQPTs disappear, decreases by enhancing the noise intensity ξ (red solid line in Fig. 6a). These findings are consistent with our expectation that the noise induces non-adiabatic transitions and a maximally mixed state ($p_k = 1/2$) does not occur at the end of quench, thus hindering the emergence of DQPTs.

As seen in the noiseless case for $J_3 < 1/2$, there are two critical modes for $v < v_c$ at which DQPTs occur. Since in the presence of noise, the p_k curve locked to the value 1/2 over a finite interval of momenta, the DQPTs region is divided into two regions: MCMs and two critical modes regions. In Fig. 6(a), the left corner of the phase diagram marked MCMs represents the MCMs region, which is separated from the two critical modes (TwCMs) region by the dashed blue line.

On the other hand, when $J_3 > 1/2$, in the noiseless phase diagram (Fig. 4) the DQPTs contains FCMs region for $v < v_{FT}$ and two critical modes region for $v_{FT} < v < v_c$. In the presence of noise, the FCMs region splits into two regions: MCMs and FCMs regions. In Fig. 6(b) the left corner of the phase diagram marked MCMs represents the MCMs region which is separated from the FCMs region by the blue dashed line.

As seen, the sweep velocity below which the system enters the MCMs region v_M (blue dashed line) increases by enhancing the noise intensity while the critical sweep velocity v_c (red solid line) reduces by increasing the noise. The numerical results indicate that the v_M converges with the critical sweep velocity v_c curve, and consequently, both curves merge into a single line for very strong noise ($\xi > 1$).
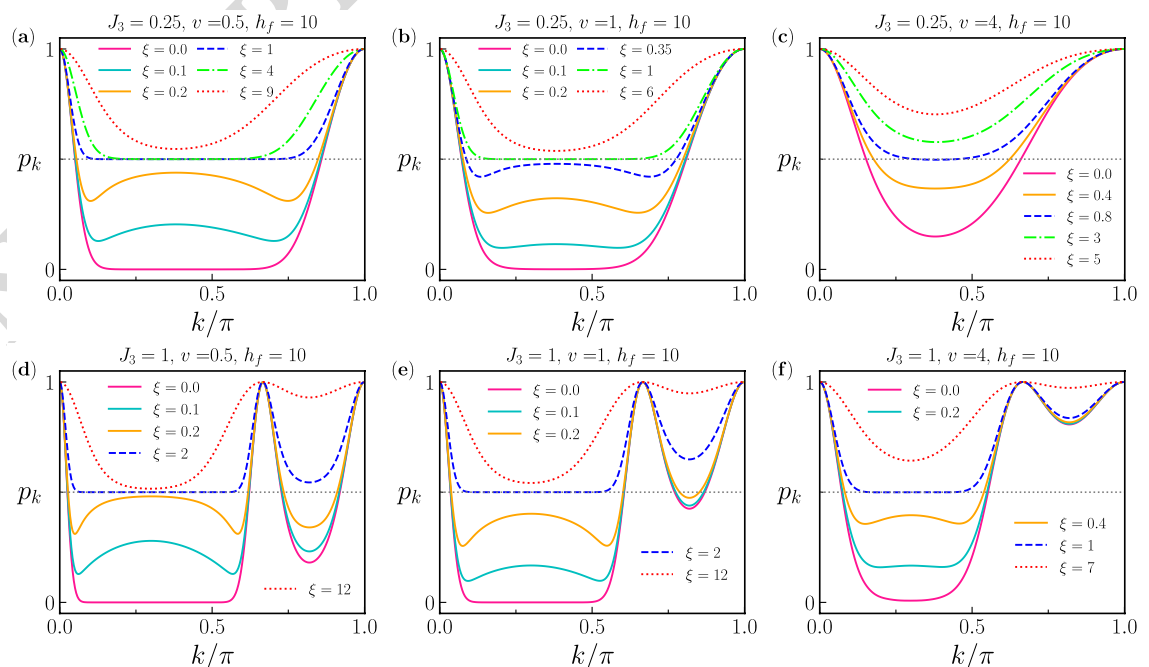

Fig. 5. (Color plot) The probability of excitations for a quench from $h_i = -10$ to $h_f = 10$ for different values of noise strength for $J_3 = 1/4$: (**a**) $v = 0.5$, (**b**) $v = 1$, and (**c**) $v = 4$, as well as for $J_3 = 1$: (**d**) $v = 0.5$, (**e**) $v = 1$, and (**f**) $v = 4$.
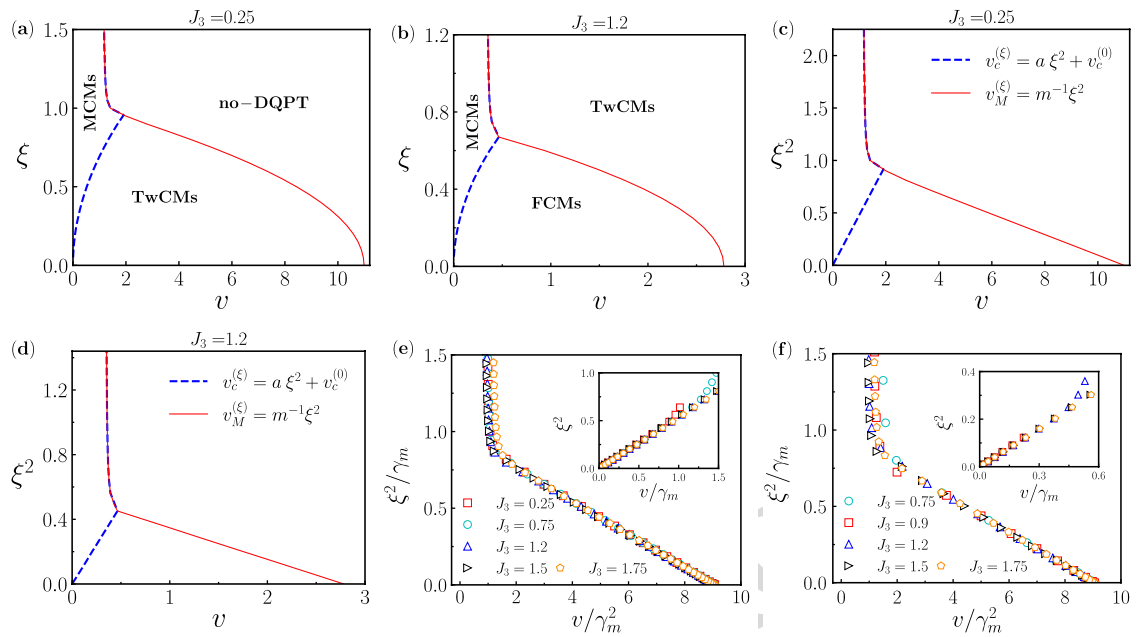
Fig. 6. (Color plot) The phase diagram in the $v - \xi$ plane for (**a**) $J_3 = 1/4$ and (**b**) $J_3 = 1.2$. The phase diagram includes two regions: DQPTs, no-DQPT regions. DQPTs region is classified into two regions: MCMs ($v < v_M$) region and two critical modes (TwCMs) region. The phase diagram in the $v - \xi^2$ plane for (**c**) $J_3 = 1/4$ and (**d**) $J_3 = 1.2$, represent linear scaling of v_c and v_M with ξ^2. (**e**) and (**f**) represent universal scaling function under which v_c curves corresponding to the different values of J_3 collapse on a single graph. Insets: the universal scaling function of v_M.

Having established that the dynamical phase diagram of the model is modified in the presence of the noise, the question then arises, does the system show any scaling and universality in the presence of noise? To this end, the critical sweep velocity v_c and v_M have been plotted in the $v - \xi^2$ plane, as shown in Fig. 6(c) and (d).

The numerical analysis shows that, the critical sweep velocity scales linearly with the square of noise intensity for both weak ($\xi \sim \mathcal{O}(10^{-2})$) and strong ($\xi \sim \mathcal{O}(10^{-1})$) noise, i.e., $v_c^{(\xi)} = a\xi^2 + v_c^{(0)}$ where $v_c^{(0)}$ represents the critical sweep velocity for the noiseless case. Additionally, a similar linear scaling is observed for v_M under both weak and strong noise conditions, given by $v_M^{(\xi)} = \xi^2/m$.

A more detailed analysis shows that the slope of lines depicted in Fig. 6(c) and (d) also scales with γ_m (see Supplemental Material Sect. 2). The numerical results demonstrate that the slops a and m scale in a power law manner with γ_m with exponent α, i.e., $\{a, m\} \propto \gamma_m^{|\alpha|}$ with $|\alpha| = 1 \pm 0.001$ for $\{a, m\}$.

A more numerical examination for both weak and strong noise illustrate a potential extrapolation for a scaling behavior of $v_c^{(\xi)}$ i.e., $v_c^{(\xi)}$ is invariant under the scaling transformation $v_c^{(\xi)} \to v_c^{(\xi)}/\gamma_m^2$ and $\xi \to \xi/\sqrt{\gamma_m}$. Moreover, the scaling function for multi-critical sweep velocity is $v_M \to v_M/\gamma_m$.

The scaling of critical sweep velocity $v_c^{(\xi)}$ corresponding to different values of J_3, for both weak and strong noise, has been illustrated in Fig. 6(e) and (f) in which all curves collapse to a single graph under the scaling function. The scaling function for v_M below which the system reveals MCMs has been also displayed in the inset of Fig. 6(e) and (f). These scaling functions are the promised universality of DQPTs in the presence of the noise. It is essential to state that we presumed the system's state following the quench to be the noise-averaged pure state, and the dynamical free energy is obtained based on this presumption; thus, the trustworthiness of our findings depends on this assumption.

Conclusions

We have studied the dynamical quantum phase transition (DQPTs) in the one dimensional Ising model with cluster interaction in the presence of the the linear time dependent transverse field. The usual symmetry in the equilibrium phase diagram of the transverse field Ising model is broken in the presence of the cluster interaction. In time-independent transverse field case, besides the two Ising like quantum phase transition points where gap closing occurs at high symmetry point in the Brillouin zone, there is a quantum phase transition between paramagnetic and cluster phases where the gap closing mode can be moved by tuning the cluster interaction strength. We have shown that, the modes which are confined between two gap closing modes (maximum transition probability ($p_k = 1$)) can be easily excited to the upper level. While the transition probability of the farthest mode from the single gap closing mode remains zero even for a sudden quench case. Consequently, DQPTs always occur for a quench that starting or ending point of the quench is limited between two critical points. In other respects there is always a critical sweep velocity above which DQPts are wiped out. Moreover, our finding also confirmed in the presence of the noisy quench while the critical sweep velocity decrease in the

presence of the noise. In addition, a surprising result occurs when the noise intensity and sweep velocity are in the same order of magnitude where the transition probability is locked to 1/2 over a finite range of momentum. In such a case, the MCMs region and consequently multi-critical time scale is induced in dynamical phase diagram. The analysis shows that the critical sweep velocity above which DQPTs disappear scales linearly with the square of noise intensify. Furthermore, the sweep velocity below which the system enters the MCMs region, increase by enhancing the noise intensity and also scales linearly with the square of noise intensity.

Data availability

All data generated or analysed during this study are included in this published article.

References

1. Hohenberg, P. C. & Halperin, B. I. Theory of dynamic critical phenomena. *Rev. Mod. Phys.* **49**, 435–479. https://doi.org/10.1103/RevModPhys.49.435 (1977).
2. Chou, T., Mallick, K. & Zia, R. K. P. Non-equilibrium statistical mechanics: From a paradigmatic model to biological transport. *Rep. Progress Phys.* **74**, 116601. https://doi.org/10.1088/0034-4885/74/11/116601 (2011).
3. Mishra, U., Prabhu, R., Sen(De), A. & Sen, U. Tuning interaction strength leads to an ergodic-nonergodic transition of quantum correlations in the anisotropic Heisenberg spin model. *Phys. Rev. A* **87**, 052318. https://doi.org/10.1103/PhysRevA.87.052318 (2013).
4. Chanda, T. et al. Static and dynamical quantum correlations in phases of an alternating-field xy model. *Phys. Rev. A* **94**, 042310. https://doi.org/10.1103/PhysRevA.94.042310 (2016).
5. Awasthi, N., Bhattacharya, S., Sen(De), A. & Sen, U. Universal quantum uncertainty relations between nonergodicity and loss of information. *Phys. Rev. A* **97**, 032103. https://doi.org/10.1103/PhysRevA.97.032103 (2018).
6. Abanin, D. A., Altman, E., Bloch, I. & Serbyn, M. Colloquium: Many-body localization, thermalization, and entanglement. *Rev. Mod. Phys.* **91**, 021001. https://doi.org/10.1103/RevModPhys.91.021001 (2019).
7. Nandkishore, R. & Huse, D. A. Many-body localization and thermalization in quantum statistical mechanics. *Ann. Rev. Condens. Matter Phys.* **6**, 15–38. https://doi.org/10.1146/annurev-conmatphys-031214-014726 (2015).
8. Wilczek, F. Quantum time crystals. *Phys. Rev. Lett.* **109**, 160401. https://doi.org/10.1103/PhysRevLett.109.160401 (2012).
9. Goldman, N. & Dalibard, J. Periodically driven quantum systems: Effective Hamiltonians and engineered Gauge fields. *Phys. Rev. X* **4**, 031027. https://doi.org/10.1103/PhysRevX.4.031027 (2014).
10. Erne, S., Bücker, R., Gasenzer, T., Berges, J. & Schmiedmayer, J. Universal dynamics in an isolated one-dimensional Bose gas far from equilibrium. *Nature* **563**, 225–229. https://doi.org/10.1038/s41586-018-0667-0 (2018).
11. Žunkovič, B., Heyl, M., Knap, M. & Silva, A. Dynamical quantum phase transitions in spin chains with long-range interactions: Merging different concepts of nonequilibrium criticality. *Phys. Rev. Lett.* **120**, 130601. https://doi.org/10.1103/PhysRevLett.120.130601 (2018).
12. Albash, T. & Lidar, D. A. Adiabatic quantum computation. *Rev. Mod. Phys.* **90**, 015002. https://doi.org/10.1103/RevModPhys.90.015002 (2018).
13. Georgescu, I. M., Ashhab, S. & Nori, F. Quantum simulation. *Rev. Mod. Phys.* **86**, 153–185. https://doi.org/10.1103/RevModPhys.86.153 (2014).
14. Polkovnikov, A., Sengupta, K., Silva, A. & Vengalattore, M. Colloquium: Nonequilibrium dynamics of closed interacting quantum systems. *Rev. Mod. Phys.* **83**, 863–883. https://doi.org/10.1103/RevModPhys.83.863 (2011).
15. Lamporesi, G., Donadello, S., Serafini, S., Dalfovo, F. & Ferrari, G. Spontaneous creation of Kibble-Zurek solitons in a Bose-Einstein condensate. *Nat. Phys.* **9**, 656–660. https://doi.org/10.1038/nphys2734 (2013).
16. Schneider, C., Porras, D. & Schaetz, T. Experimental quantum simulations of many-body physics with trapped ions. *Rep. Progress Phys.* **75**, 024401. https://doi.org/10.1088/0034-4885/75/2/024401 (2012).
17. Jotzu, G. et al. Experimental realization of the topological Haldane model with ultracold fermions. *Nature* **515**, 237–240. https://doi.org/10.1038/nature13915 (2014).
18. Daley, A. J., Pichler, H., Schachenmayer, J. & Zoller, P. Measuring entanglement growth in quench dynamics of bosons in an optical lattice. *Phys. Rev. Lett.* **109**, 020505. https://doi.org/10.1103/PhysRevLett.109.020505 (2012).
19. Schreiber, M. et al. Observation of many-body localization of interacting fermions in a quasirandom optical lattice. *Science* **349**, 842–845. https://doi.org/10.1126/science.aaa7432 (2015).
20. Choi, J.-Y. et al. Exploring the many-body localization transition in two dimensions. *Science* **352**, 1547–1552. https://doi.org/10.1126/science.aaf8834 (2016).
21. Fläschner, N. et al. Observation of dynamical vortices after quenches in a system with topology. *Nat. Phys.* **14**, 265. https://doi.org/10.1038/s41567-017-0013-8 (2017).
22. Jurcevic, P. et al. Direct observation of dynamical quantum phase transitions in an interacting many-body system. *Phys. Rev. Lett.* **119**, 080501. https://doi.org/10.1103/PhysRevLett.119.080501 (2017).
23. Martinez, E. A. et al. Real-time dynamics of lattice gauge theories with a few-qubit quantum computer. *Nature* **534**, 516–519 (2016).
24. Neyenhuis, B. et al. Observation of prethermalization in long-range interacting spin chains. *Sci. Adv.* **3**, e1700672. https://doi.org/10.1126/sciadv.1700672 (2017).
25. Smith, J. et al. Many-body localization in a quantum simulator with programmable random disorder. *Nat. Phys.* **12**, 907–911. https://doi.org/10.1038/nphys3783 (2016).
26. Yang, K. et al. Floquet dynamical quantum phase transitions. *Phys. Rev. B* **100**, 085308. https://doi.org/10.1103/PhysRevB.100.085308 (2019).
27. Guo, X.-Y. et al. Observation of a dynamical quantum phase transition by a superconducting qubit simulation. *Phys. Rev. Appl.* **11**, 044080. https://doi.org/10.1103/PhysRevApplied.11.044080 (2019).
28. Wang, K. et al. Simulating dynamic quantum phase transitions in photonic quantum walks. *Phys. Rev. Lett.* **122**, 020501. https://doi.org/10.1103/PhysRevLett.122.020501 (2019).
29. Xu, X.-Y. et al. Measuring a dynamical topological order parameter in quantum walks. *Light Sci. Appl.* **9**, 1. https://doi.org/10.1038/s41377-019-0237-8 (2020).
30. Horsthemke, W. Noise induced transitions. In *Non-Equilibrium Dynamics in Chemical Systems, 150–160 (Springer* (eds Vidal, C. & Pacault, A.) (Berlin Heidelberg, Berlin, Heidelberg, 1984).
31. Zoller, P., Alber, G. & Salvador, R. ac stark splitting in intense stochastic driving fields with gaussian statistics and non-lorentzian line shape. *Phys. Rev. A* **24**, 398–410. https://doi.org/10.1103/PhysRevA.24.398 (1981).
32. Chen, X. et al. Fast optimal frictionless atom cooling in harmonic traps: Shortcut to adiabaticity. *Phys. Rev. Lett.* **104**, 063002. https://doi.org/10.1103/PhysRevLett.104.063002 (2010).

33. Doria, P., Calarco, T. & Montangero, S. Optimal control technique for many-body quantum dynamics. *Phys. Rev. Lett.* **106**, 190501. https://doi.org/10.1103/PhysRevLett.106.190501 (2011).
34. Pichler, H., Schachenmayer, J., Simon, J., Zoller, P. & Daley, A. J. Noise- and disorder-resilient optical lattices. *Phys. Rev. A* **86**, 051605. https://doi.org/10.1103/PhysRevA.86.051605 (2012).
35. Heyl, M., Polkovnikov, A. & Kehrein, S. Dynamical quantum phase transitions in the transverse-field Ising model. *Phys. Rev. Lett.* **110**, 135704. https://doi.org/10.1103/PhysRevLett.110.135704 (2013).
36. Hey, M. & Budich, J. C. Dynamical topological quantum phase transitions for mixed states. *Phys. Rev. B* **96**, 180304. https://doi.org/10.1103/PhysRevB.96.180304 (2017).
37. Heyl, M. Dynamical quantum phase transitions: A review. *Rep. Progress Phys.* **81**, 054001. https://doi.org/10.1088/1361-6633/aaaf9a (2018).
38. Andraschko, F. & Sirker, J. Dynamical quantum phase transitions and the loschmidt echo: A transfer matrix approach. *Phys. Rev. B* **89**, 125120. https://doi.org/10.1103/PhysRevB.89.125120 (2014).
39. Karrasch, C. & Schuricht, D. Dynamical phase transitions after quenches in nonintegrable models. *Phys. Rev. B* **87**, 195104. https://doi.org/10.1103/PhysRevB.87.195104 (2013).
40. Jafari, R. Dynamical quantum phase transition and quasi particle excitation. *Sci. Rep.* **9**, 2871. https://doi.org/10.1038/s41598-019-39595-3 (2019).
41. Mondal, D. & Nag, T. Anomaly in the dynamical quantum phase transition in a non-hermitian system with extended gapless phases. *Phys. Rev. B* **106**, 054308. https://doi.org/10.1103/PhysRevB.106.054308 (2022).
42. Mendoza-Arenas, J. J. Dynamical quantum phase transitions in the one-dimensional extended Fermi–Hubbard model. *J. Stat. Mech. Theory Exp.* **2022**, 043101. https://doi.org/10.1088/1742-5468/ac6031 (2022).
43. Sedlmayr, N., Fleischhauer, M. & Sirker, J. Fate of dynamical phase transitions at finite temperatures and in open systems. *Phys. Rev. B* **97**, 045147. https://doi.org/10.1103/PhysRevB.97.045147 (2018).
44. Sedlmayr, N., Jaeger, P., Maiti, M. & Sirker, J. Bulk-boundary correspondence for dynamical phase transitions in one-dimensional topological insulators and superconductors. *Phys. Rev. B* **97**, 064304. https://doi.org/10.1103/PhysRevB.97.064304 (2018).
45. Khatun, A. & Bhattacharjee, S. M. Boundaries and unphysical fixed points in dynamical quantum phase transitions. *Phys. Rev. Lett.* **123**, 160603. https://doi.org/10.1103/PhysRevLett.123.160603 (2019).
46. Ding, C. Dynamical quantum phase transition from a critical quantum quench. *Phys. Rev. B* **102**, 060409. https://doi.org/10.1103/PhysRevB.102.060409 (2020).
47. Rossi, L. & Dolcini, F. Nonlinear current and dynamical quantum phase transitions in the flux-quenched Su-Schrieffer-Heeger model. *Phys. Rev. B* **106**, 045410. https://doi.org/10.1103/PhysRevB.106.045410 (2022).
48. Khan, N. A., Wang, P., Jan, M. & Xianlong, G. Anomalous correlation-induced dynamical quantum phase transitions. *Sci. Rep.* **13**, 9470. https://doi.org/10.1038/s41598-023-36564-9 (2023).
49. Vajna, S. & Dóra, B. Disentangling dynamical phase transitions from equilibrium phase transitions. *Phys. Rev. B* **89**, 161105. https://doi.org/10.1103/PhysRevB.89.161105 (2014).
50. Porta, S., Cavaliere, F., Sassetti, M. & Traverso Ziani, N. Topological classification of dynamical quantum phase transitions in the xy chain. *Sci. Rep.* **10**, 12766. https://doi.org/10.1038/s41598-020-69621-8 (2020).
51. Ye, S., Zhou, Z., Khan, N. A. & Xianlong, G. Energy-dependent dynamical quantum phase transitions in quasicrystals. *Phys. Rev. A* **109**, 043319. https://doi.org/10.1103/PhysRevA.109.043319 (2024).
52. Ye, S., Khan, N. A. & Sajid, M. Disentangling connection between static and dynamical phase transitions. *Phys. Rev. A* **111**, 042208. https://doi.org/10.1103/PhysRevA.111.042208 (2025).
53. Jafari, R., Johannesson, H., Langari, A. & Martin-Delgado, M. A. Quench dynamics and zero-energy modes: The case of the Creutz model. *Phys. Rev. B* **99**, 054302. https://doi.org/10.1103/PhysRevB.99.054302 (2019).
54. Jafari, R. & Johannesson, H. Loschmidt echo revivals: Critical and noncritical. *Phys. Rev. Lett.* **118**, 015701. https://doi.org/10.1103/PhysRevLett.118.015701 (2017).
55. Najafi, K., Rajabpour, M. A. & Viti, J. Return amplitude after a quantum quench in the XY chain. *J. Stat. Mech. Theory Exp.* **2019**, 083102. https://doi.org/10.1088/1742-5468/ab3413 (2019).
56. Sadrzadeh, M., Jafari, R. & Langari, A. Dynamical topological quantum phase transitions at criticality. *Phys. Rev. B* **103**, 144305. https://doi.org/10.1103/PhysRevB.103.144305 (2021).
57. Wong, C. Y. & Yu, W. C. Loschmidt amplitude spectrum in dynamical quantum phase transitions. *Phys. Rev. B* **105**, 174307. https://doi.org/10.1103/PhysRevB.105.174307 (2022).
58. Rylands, C., Yuzbashyan, E. A., Gurarie, V., Zabalo, A. & Galitski, V. Loschmidt echo of far-from-equilibrium fermionic superfluids. *Annals Phys.* **435**, 168554. https://doi.org/10.1016/j.aop.2021.168554 (2021).
59. Abdi, M. Dynamical quantum phase transition in Bose-Einstein condensates. *Phys. Rev. B* **100**, 184310. https://doi.org/10.1103/PhysRevB.100.184310 (2019).
60. Uhrich, P., Defenu, N., Jafari, R. & Halimeh, J. C. Out-of-equilibrium phase diagram of long-range superconductors. *Phys. Rev. B* **101**, 245148. https://doi.org/10.1103/PhysRevB.101.245148 (2020).
61. Wong, C. Y., Cheraghi, H. & Yu, W. C. Quantum spin fluctuations in dynamical quantum phase transitions. *Phys. Rev. B* **108**, 064305. https://doi.org/10.1103/PhysRevB.108.064305 (2023).
62. Sacramento, P. D. & Yu, W. C. Distribution of fisher zeros in dynamical quantum phase transitions of two-dimensional topological systems. *Phys. Rev. B* **109**, 134301. https://doi.org/10.1103/PhysRevB.109.134301 (2024).
63. Zhou, B., Zeng, Y. & Chen, S. Exact zeros of the Loschmidt echo and quantum speed limit time for the dynamical quantum phase transition in finite-size systems. *Phys. Rev. B* **104**, 094311. https://doi.org/10.1103/PhysRevB.104.094311 (2021).
64. Vanhala, T. I. & Ojanen, T. Theory of the Loschmidt echo and dynamical quantum phase transitions in disordered fermi systems. *Phys. Rev. Res.* **5**, 033178. https://doi.org/10.1103/PhysRevResearch.5.033178 (2023).
65. Mondal, D. & Nag, T. Finite-temperature dynamical quantum phase transition in a non-hermitian system. *Phys. Rev. B* **107**, 184311. https://doi.org/10.1103/PhysRevB.107.184311 (2023).
66. Cao, K., Li, W., Zhong, M. & Tong, P. Influence of weak disorder on the dynamical quantum phase transitions in the anisotropic xy chain. *Phys. Rev. B* **102**, 014207. https://doi.org/10.1103/PhysRevB.102.014207 (2020).
67. Masłowski, T. & Sedlmayr, N. Dynamical bulk-boundary correspondence and dynamical quantum phase transitions in higher-order topological insulators. *Phys. Rev. B* **108**, 094306. https://doi.org/10.1103/PhysRevB.108.094306 (2023).
68. Wrześniewski, K., Weymann, I., Sedlmayr, N. & Domański, T. Dynamical quantum phase transitions in a mesoscopic superconducting system. *Phys. Rev. B* **105**, 094514. https://doi.org/10.1103/PhysRevB.105.094514 (2022).
69. Masłowski, T. & Sedlmayr, N. Quasiperiodic dynamical quantum phase transitions in multiband topological insulators and connections with entanglement entropy and fidelity susceptibility. *Phys. Rev. B* **101**, 014301. https://doi.org/10.1103/PhysRevB.101.014301 (2020).
70. Zeng, Y., Zhou, B. & Chen, S. Dynamical singularity of the rate function for quench dynamics in finite-size quantum systems. *Phys. Rev. B* **107**, 134302. https://doi.org/10.1103/PhysRevB.107.134302 (2023).
71. Stumper, S., Thoss, M. & Okamoto, J. Interaction-driven dynamical quantum phase transitions in a strongly correlated bosonic system. *Phys. Rev. Res.* **4**, 013002. https://doi.org/10.1103/PhysRevResearch.4.013002 (2022).
72. Yu, W. C., Sacramento, P. D., Li, Y. C. & Lin, H.-Q. Correlations and dynamical quantum phase transitions in an interacting topological insulator. *Phys. Rev. B* **104**, 085104. https://doi.org/10.1103/PhysRevB.104.085104 (2021).

73. Vijayan, V. et al. Topological dynamical quantum phase transition in a quantum skyrmion phase. *Phys. Rev. B* **107**, L100419. https://doi.org/10.1103/PhysRevB.107.L100419 (2023).
74. Yu, X.-J. Dynamical phase transition and scaling in the chiral clock potts chain. *Phys. Rev. A* **108**, 062215. https://doi.org/10.1103/PhysRevA.108.062215 (2023).
75. Bhattacharjee, S. M. Complex dynamics approach to dynamical quantum phase transitions: The potts model. *Phys. Rev. B* **109**, 035130. https://doi.org/10.1103/PhysRevB.109.035130 (2024).
76. Lakkaraju, L. G. C., Haldar, S. K. & Sen(De), A. Predicting a topological quantum phase transition from dynamics via multisite entanglement. *Phys. Rev. A* **109**, 022436. https://doi.org/10.1103/PhysRevA.109.022436 (2024).
77. Zamani, S., Naji, J., Jafari, R. & Langari, A. Scaling and universality at ramped quench dynamical quantum phase transitions. *J. Phys. Condens. Matter* **36**, 355401. https://doi.org/10.1088/1361-648X/ad4df9 (2024).
78. Mishra, U., Jafari, R. & Akbari, A. Disordered Kitaev chain with long-range pairing: Loschmidt echo revivals and dynamical phase transitions. *J. Phys. A Math. Theor.* **53**, 375301. https://doi.org/10.1088/1751-8121/ab97de (2020).
79. Haldar, S., Roy, S., Chanda, T., Sen(De), A. & Sen, U. Multipartite entanglement at dynamical quantum phase transitions with nonuniformly spaced criticalities. *Phys. Rev. B* **101**, 224304. https://doi.org/10.1103/PhysRevB.101.224304 (2020).
80. Halimeh, J. C., Trapin, D., Van Damme, M. & Heyl, M. Local measures of dynamical quantum phase transitions. *Phys. Rev. B* **104**, 075130. https://doi.org/10.1103/PhysRevB.104.075130 (2021).
81. Corps, A. L., Relaño, A. & Halimeh, J. C. Unifying finite-temperature dynamical and excited-state quantum phase transitions. *Phys. Rev. Res.* **6**, 043080. https://doi.org/10.1103/PhysRevResearch.6.043080 (2024).
82. Van Damme, M., Desaules, J.-Y., Papić, Z. & Halimeh, J. C. Anatomy of dynamical quantum phase transitions. *Phys. Rev. Res.* **5**, 033090. https://doi.org/10.1103/PhysRevResearch.5.033090 (2023).
83. Halimeh, J. C., Van Damme, M., Guo, L., Lang, J. & Hauke, P. Dynamical phase transitions in quantum spin models with antiferromagnetic long-range interactions. *Phys. Rev. B* **104**, 115133. https://doi.org/10.1103/PhysRevB.104.115133 (2021).
84. Zamani, S., Jafari, R. & Langari, A. Floquet dynamical quantum phase transition in the extended xy model: Nonadiabatic to adiabatic topological transition. *Phys. Rev. B* **102**, 144306. https://doi.org/10.1103/PhysRevB.102.144306 (2020).
85. Kosior, A. & Sacha, K. Dynamical quantum phase transitions in discrete time crystals. *Phys. Rev. A* **97**, 053621. https://doi.org/10.1103/PhysRevA.97.053621 (2018).
86. Jafari, R. & Akbari, A. Floquet dynamical phase transition and entanglement spectrum. *Phys. Rev. A* **103**, 012204. https://doi.org/10.1103/PhysRevA.103.012204 (2021).
87. Kosior, A., Syrwid, A. & Sacha, K. Dynamical quantum phase transitions in systems with broken continuous time and space translation symmetries. *Phys. Rev. A* **98**, 023612. https://doi.org/10.1103/PhysRevA.98.023612 (2018).
88. Naji, J., Jafari, M., Jafari, R. & Akbari, A. Dissipative floquet dynamical quantum phase transition. *Phys. Rev. A* **105**, 022220. https://doi.org/10.1103/PhysRevA.105.022220 (2022).
89. Jafari, R., Akbari, A., Mishra, U. & Johannesson, H. Floquet dynamical quantum phase transitions under synchronized periodic driving. *Phys. Rev. B* **105**, 094311. https://doi.org/10.1103/PhysRevB.105.094311 (2022).
90. Naji, J., Jafari, R., Zhou, L. & Langari, A. Engineering floquet dynamical quantum phase transitions. *Phys. Rev. B* **106**, 094314. https://doi.org/10.1103/PhysRevB.106.094314 (2022).
91. Budich, J. C. & Heyl, M. Dynamical topological order parameters far from equilibrium. *Phys. Rev. B* **93**, 085416. https://doi.org/10.1103/PhysRevB.93.085416 (2016).
92. Bhattacharya, U., Bandyopadhyay, S. & Dutta, A. Mixed state dynamical quantum phase transitions. *Phys. Rev. B* **96**, 180303. https://doi.org/10.1103/PhysRevB.96.180303 (2017).
93. Nie, X. et al. Experimental observation of equilibrium and dynamical quantum phase transitions via out-of-time-ordered correlators. *Phys. Rev. Lett.* **124**, 250601. https://doi.org/10.1103/PhysRevLett.124.250601 (2020).
94. Tian, T. et al. Observation of dynamical quantum phase transitions with correspondence in an excited state phase diagram. *Phys. Rev. Lett.* **124**, 043001. https://doi.org/10.1103/PhysRevLett.124.043001 (2020).
95. Jafari, R., Langari, A., Eggert, S. & Johannesson, H. Dynamical quantum phase transitions following a noisy quench. *Phys. Rev. B* **109**, L180303. https://doi.org/10.1103/PhysRevB.109.L180303 (2024).
96. Baghran, R., Jafari, R. & Langari, A. Competition of long-range interactions and noise at a ramped quench dynamical quantum phase transition: The case of the long-range pairing Kitaev chain. *Phys. Rev. B* **110**, 064302. https://doi.org/10.1103/PhysRevB.110.064302 (2024).
97. Dutta, A., Rahmani, A. & del Campo, A. Anti-Kibble-Zurek behavior in crossing the quantum critical point of a thermally isolated system driven by a noisy control field. *Phys. Rev. Lett.* **117**, 080402. https://doi.org/10.1103/PhysRevLett.117.080402 (2016).
98. Bando, Y. et al. Probing the universality of topological defect formation in a quantum annealer: Kibble-Zurek mechanism and beyond. *Phys. Rev. Res.* **2**, 033369. https://doi.org/10.1103/PhysRevResearch.2.033369 (2020).
99. Chenu, A., Beau, M., Cao, J. & del Campo, A. Quantum simulation of generic many-body open system dynamics using classical noise. *Phys. Rev. Lett.* **118**, 140403. https://doi.org/10.1103/PhysRevLett.118.140403 (2017).
100. Jafari, R., Asadian, A., Abdi, M. & Akbari, A. Dynamics of decoherence in a noisy driven environment. *Sci. Rep.* **15**, 1–12. https://doi.org/10.1038/s41598-025-00815-8 (2025).
101. Sadeghizade, S., Jafari, R. & Langari, A. Anti-Kibble-Zurek behavior in the quantum xy spin-$\frac{1}{2}$ chain driven by correlated noisy magnetic field and anisotropy. *Phys. Rev. B* **111**, 104310. https://doi.org/10.1103/PhysRevB.111.104310 (2025).
102. Verga, A. D. Entanglement dynamics and phase transitions of the floquet cluster spin chain. *Phys. Rev. B* **107**, 085116. https://doi.org/10.1103/PhysRevB.107.085116 (2023).
103. Son, W. et al. Quantum phase transition between cluster and antiferromagnetic states. *Europhys. Lett.* **95**, 50001. https://doi.org/10.1209/0295-5075/95/50001 (2011).
104. Smacchia, P. et al. Statistical mechanics of the cluster Ising model. *Phys. Rev. A* **84**, 022304. https://doi.org/10.1103/PhysRevA.84.022304 (2011).
105. Niu, Y. et al. Majorana zero modes in a quantum Ising chain with longer-ranged interactions. *Phys. Rev. B* **85**, 035110. https://doi.org/10.1103/PhysRevB.85.035110 (2012).
106. Montes, S. & Hamma, A. Phase diagram and quench dynamics of the cluster-xy spin chain. *Phys. Rev. E* **86**, 021101. https://doi.org/10.1103/PhysRevE.86.021101 (2012).
107. Kopp, A. & Chakravarty, S. Criticality in correlated quantum matter. *Nat. Phys.* **1**, 53–56. https://doi.org/10.1038/nphys105 (2005).
108. Hirsch, J. E. & Mazenko, G. F. Renormalization-group transformation for quantum lattice systems at zero temperature. *Phys. Rev. B* **19**, 2656–2663. https://doi.org/10.1103/PhysRevB.19.2656 (1979).
109. Doherty, A. C. & Bartlett, S. D. Identifying phases of quantum many-body systems that are universal for quantum computation. *Phys. Rev. Lett.* **103**, 020506. https://doi.org/10.1103/PhysRevLett.103.020506 (2009).
110. Yu, X.-J. & Li, W.-L. Fidelity susceptibility at the Lifshitz transition between the noninteracting topologically distinct quantum critical points. *Phys. Rev. B* **110**, 045119. https://doi.org/10.1103/PhysRevB.110.045119 (2024).
111. Ding, C. Phase transitions of a cluster Ising model. *Phys. Rev. E* **100**, 042131. https://doi.org/10.1103/PhysRevE.100.042131 (2019).
112. Ansari, S., Jafari, R., Akbari, A. & Abdi, M. Scaling and universality at noisy quench dynamical quantum phase transitions. arXiv preprint arXiv:2506.14355 (2025).

113. Sharma, S., Divakaran, U., Polkovnikov, A. & Dutta, A. Slow quenches in a quantum Ising chain: Dynamical phase transitions and topology. *Phys. Rev. B* **93**, 144306. https://doi.org/10.1103/PhysRevB.93.144306 (2016).
114. Dóra, B., Pollmann, F., Fortágh, J. & Zaránd, G. Loschmidt echo and the many-body orthogonality catastrophe in a qubit-coupled Luttinger liquid. *Phys. Rev. Lett.* **111**, 046402. https://doi.org/10.1103/PhysRevLett.111.046402 (2013).
115. Bhattacharjee, S. & Dutta, A. Dynamical quantum phase transitions in extended transverse Ising models. *Phys. Rev. B* **97**, 134306. https://doi.org/10.1103/PhysRevB.97.134306 (2018).
116. Becker, C. et al. Ultracold quantum gases in triangular optical lattices. *New J. Phys.* **12**, 065025. https://doi.org/10.1088/1367-2630/12/6/065025 (2010).
117. Briegel, H. J. & Raussendorf, R. Persistent entanglement in arrays of interacting particles. *Phys. Rev. Lett.* **86**, 910–913. https://doi.org/10.1103/PhysRevLett.86.910 (2001).
118. Pachos, J. K. & Plenio, M. B. Three-spin interactions in optical lattices and criticality in cluster hamiltonians. *Phys. Rev. Lett.* **93**, 056402. https://doi.org/10.1103/PhysRevLett.93.056402 (2004).
119. Skrøvseth, S. O. & Bartlett, S. D. Phase transitions and localizable entanglement in cluster-state spin chains with Ising couplings and local fields. *Phys. Rev. A* **80**, 022316. https://doi.org/10.1103/PhysRevA.80.022316 (2009).
120. Lieb, E., Schultz, T. & Mattis, D. Two soluble models of an antiferromagnetic chain. *Annals Phys.* **16**, 407–466. https://doi.org/10.1016/0003-4916(61)90115-4 (1961).
121. Jafari, R. Thermodynamic properties of the one-dimensional extended quantum compass model in the presence of a transverse field. *Eur. Phys. J. B* **85**, 167. https://doi.org/10.1140/epjb/e2012-20682-5 (2012).
122. Divakaran, U. & Dutta, A. The effect of the three-spin interaction and the next nearest neighbor interaction on the quenching dynamics of a transverse ising model. *J. Stat. Mech. Theory Exp.* **2007**, P11001. https://doi.org/10.1088/1742-5468/2007/11/P11001 (2007).
123. Bunder, J. E. & McKenzie, R. H. Effect of disorder on quantum phase transitions in anisotropic xy spin chains in a transverse field. *Phys. Rev. B* **60**, 344–358. https://doi.org/10.1103/PhysRevB.60.344 (1999).
124. Vitanov, N. V. Transition times in the Landau-Zener model. *Phys. Rev. A* **59**, 988–994. https://doi.org/10.1103/PhysRevA.59.988 (1999).
125. Vitanov, N. V. & Garraway, B. M. Landau-Zener model: Effects of finite coupling duration. *Phys. Rev. A* **53**, 4288–4304. https://doi.org/10.1103/PhysRevA.53.4288 (1996).
126. Erdelyi, A., Magnus, W., Oberhettinger, F. & Tricomi, F. Higher transcendental functions, vol. 1 mcgraw-hill. *New York* **7954** (1953).
127. Abramowitz, M., Stegun, I. A. & Romer, R. H. Handbook of mathematical functions with formulas, graphs, and mathematical tables. *Am. J. Phys.* **56**, 958–958. https://doi.org/10.1119/1.15378 (1988).
128. Gao, Z.-P., Zhang, D.-W., Yu, Y. & Zhu, S.-L. Anti-Kibble-Zurek behavior of a noisy transverse-field XY chain and its quantum simulation with two-level systems. *Phys. Rev. B* **95**, 224303. https://doi.org/10.1103/PhysRevB.95.224303 (2017).
129. Ai, M.-Z. et al. Experimental verification of anti-Kibble-Zurek behavior in a quantum system under a noisy control field. *Phys. Rev. A* **103**, 012608. https://doi.org/10.1103/PhysRevA.103.012608 (2021).
130. Singh, M. & Gangadharaiah, S. Driven quantum spin chain in the presence of noise: Anti-Kibble-Zurek behavior. *Phys. Rev. B* **104**, 064313. https://doi.org/10.1103/PhysRevB.104.064313 (2021).
131. Luczka, J. Quantum open systems in a two-state stochastic reservoir. *Czechoslovak J. Phys.* **41**, 289–292. https://doi.org/10.1007/BF01598768 (1991).
132. Budini, A. A. Non-Markovian Gaussian dissipative stochastic wave vector. *Phys. Rev. A* **63**, 012106. https://doi.org/10.1103/PhysRevA.63.012106 (2000).
133. Costa-Filho, J. I. et al. Enabling quantum non-Markovian dynamics by injection of classical colored noise. *Phys. Rev. A* **95**, 052126. https://doi.org/10.1103/PhysRevA.95.052126 (2017).
134. Kiely, A. Exact classical noise master equations: Applications and connections. *Europhys. Lett.* **134**, 10001. https://doi.org/10.1209/0295-5075/134/10001 (2021).

Acknowledgements

Author contributions

All authors (S. Kheiri, R. Jafari, S. Mahdavifar, E. Nedaaee Oskoee, and A. Akbari) contribute equally to the idea generation and paper writing process.

Funding

Declarations

Conflict of interest

The authors declare that they have no conflict of interest.

Additional information

Supplementary Information The online version contains supplementary material available at https://doi.org/10.1038/s41598-025-26732-4.

Correspondence and requests for materials should be addressed to R.J.

Reprints and permissions information is available at www.nature.com/reprints.

Publisher's note Springer Nature remains neutral with regard to jurisdictional claims in published maps and institutional affiliations.